Macromodeling of Operational Amplifier's Power Supply Rejection Ratio Effects

Elena Dikova Shoikova, Ivailo Milanov Pandiev
Technical University of Sofia.
E-mail: shoikova@vmei.acad.bg, WWW: http://www.demlab.vmei.acad.bg

Abstract. *In this paper we present the operational amplifier (op amp) simulation model developments aimed at improving the scope and accuracy of the power supply rejection ratio versus represented by the PSpice macromodels. Generally speaking, simulation modeling has been used to tackle a range of design problems leading to improvements in efficiency, reduced costs and increased profitability. Here we have focused our attention on the method of building simulation models employed by professional ECAD software. The new simulation models are realized by modifying the op amp macromodels featuring different levels of complexity by adding new elements / stages to the respective equivalent circuit. The improved macromodels have been validated by comparing simulation results with parameter values from IC data sheets, namely by considering the average values of the parameters provided by manufacturers. The new op amp macromodels are defined as sub-circuits compatible with formats used by the analog-digital simulator PSpice A/D.*

1. Introduction

The need analysis performed has shown that in modern IC designs, analog and digital functions are joined together on the same chip, and correspondingly an interaction is likely to occur between circuit components. This interaction will consist of spikes that are generated by clocks (in digital components or in switched-capacitor circuits), output drives, etc. Spikes are generated on supply lines, ground, or substrate. Those spikes can be easily coupled to the analog circuits. One of the important characteristics of modern analog units is their insensitivity to spikes on supply lines. This feature is expressed by their Power Supply Rejection Ratios (*PSRR*s). A specific difficulty associated with *PSRR* is that high values of *PSRR* can be more easily obtained at low frequencies while it is much harder to do this at high frequencies. However, it is especially at the high frequencies that the high *PSRR* value is required. Spikes on power supply lines are characterized by short duration, and thus contain a large number of high frequency components. As a consequence, a high *PSRR* value is required at intermediate and high frequencies only. In most cases the frequency dependence of *PSRR* is being represented by using first- or second-order transfer functions determined by real poles or a real pole/zero pair. As a response to these needs we have developed the op amp simulation *PSpice*-macromodels aimed at improving the scope and accuracy of the *PSRR* versus frequency and accounting for its thermal drift.

Nowadays there are more than 1600 *PSpice* op amp macromodels represented in four different levels of complexity [1]. In the input stage of these macromodels voltage-controlled voltage-sources E_{GND} (for levels 1 and 2) and E_{RFF} (or E_H) (for level 3) measure the supply voltages and provide a stiff point between the rails to which other stages are referenced [1]. It has been noted that in all existing macromodels (1, 2 and 3 levels of complexity) the invariable coefficients of the controlled sources E_{GND} and E_{RFF} (or E_H) were chosen empirically. If the supply rails are asymmetrical, the voltage at node 99 (for levels 1 and 2) or 98 (for level 3) will be different from $0V$. Then the values of open-loop voltage gain A_{VD}, bandwidth B_1 and other parameters of op amp models will be changed. Thus, it

will not be possible to represent the actual behavior of *PSRR*s by using those elements (E_{GND} and E_{RFF}/E_H). The macromodel proposed by Hu (referred to as the HLC macromodel) [4] is well suited for predicting all main terminal characteristics of op amps and takes into account the DC value of Power Supply Rejection. However, the HLC model has not been included in *PSpice* libraries. Using a combination of simplification and build-up methods [1, 2, and 3] has developed contemporary op amp macromodels. They are more accurate and take account of some of the second-order effects. So, the *PSRR* and power supply ripple rejection ratios are presented in Texas Instruments (TI) macromodels [1, 2]. There are small groups of models (105 devices) in which *PSRR* vs. frequency is simulated as a one-pole system at room temperature only. However, the validation of these macromodels performed by comparing the simulation results with corresponding values from op amp data sheets shows an error for *PSRR* higher than 50 %. Also, the difference between positive and negative *PSRR*s has not been accounted for by TI macromodels. Therefore, the macromodels available cannot provide fully adequate representation of the op amp behavior when exist voltage spikes on supply lines.

2. Building the op amp macromodels accounting for the frequency dependence of the *PSRR*

By applying the method of step-like building that is a basic tool for incorporating second-order effects, it is possible to develop further the existing macromodels towards adequate presentation of the frequency dependence of the Power Supply Rejection Ratio. Besides, the analysis of graphic plots has shown that in most cases these characteristics could be approximated by transfer functions of first or second orders. The Power Supply Rejection Ratio *PSRR* is defined as the absolute value of the ratio of the change in input voltage of asymmetry to the change in the op amp supply voltages that has caused that change. Normally, technical data sheets provided by IC-manufacturers contain information regarding the frequency dependence of The Power Supply Rejection Ratio *PSRR* that could be used in modeling the real op amps.

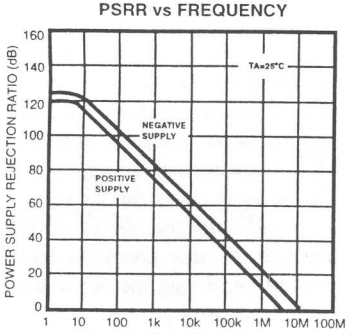

Fig. 1. OP-27 *PSRR* effects

2.1. One-pole approximation of the frequency characteristic of PSRR

Typical logarithmic characteristics of *PSRR* depending on the frequency for the positive and negative supply voltages are shown in Fig. 1 (*Analog Devices* OP-27). The different maximal values of $PSRR^{+}_{DC} = 1.10^{6}$ and $PSRR^{-}_{DC} = 1{,}7782.10^{6}$ have been measured at frequency $1\,Hz$, and the boundary frequencies at the level of $-3dB$ are $f_{P(PSR^{+})} = 6Hz$ and $f_{P(PSR^{-})} = 11{,}24Hz$, respectively. In transition area the slope of characteristics is $-20dB/dec$. Therefore, providing an accuracy sufficient for practical purposes, in this case the frequency characteristic of *PSRR* can be presented as a low-frequency function. A ddevelopment of the op amp macromodels of first, second, and third levels has been proposed on the basis of the definition of *PSRR* and analysis of data-sheet values. As it is shown in Fig. 2, the equivalent

circuits of existing macromodels of different levels of complexity are modified by adding new elements and stages as follows. A linear two-port dependent voltage-controlled voltage supply E_{PSR} is connected to the input circuit of the macromodel, creating a new node 205. The state of this new node will have to follow the change in the input voltage of asymmetry, modeling PSSR. This can be performed by appropriately selecting the two controlling voltages that are respectively determined by the positive and negative supply voltages V^+ and V^-. For this purpose new stages consisting of dependent current sources, G_{PSR^+} and G_{PSR^-}, controlled by supply voltages and various frequency-determining RL-groups are introduced into the equivalent circuits of different macromodels. The source G_{PSR^+} presets the voltage at node 201 that depends on the ripples of supply voltage $(V^+ \pm \Delta V^+)$, and G_{PSR^-} forms the voltage at node 202 being dependent on ripples in the negative supply voltage $(V^- \pm \Delta V^-)$. A sufficient degree of accuracy for the purposes of modeling has been provided by choosing G_{PSR^+} and G_{PSR^-} as linear one-port sources having the following characteristic equations:

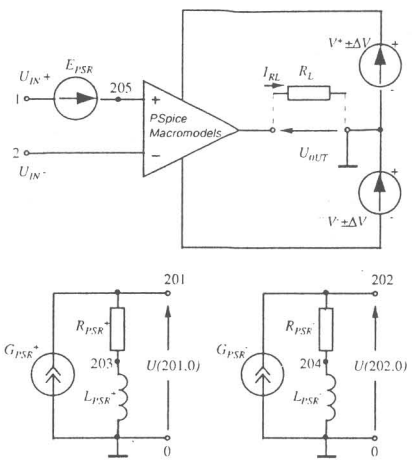

Fig. 2. Modified circuit op amp of macromodel for representing one-pole approximation of the frequency characteristic of *PSRR*

(1a) $I(G_{PSR^+}) = k_{1.GPSR^+}\left(V^+ \pm \Delta V^+\right)$, and

(1b) $I(G_{PSR^-}) = k_{1.GPSR^-}\left(V^- \pm \Delta V^-\right)$,

respectively.

The currents thus generated, $I(G_{PSR^+})$ and $I(G_{PSR^-})$, will flow through the arms consisting of the elements R_{PSR^+}, L_{PSR^+} and R_{PSR^-}, L_{PSR^-}, towards the internal ground. In such a way the voltages $U(201,0)$ and $U(202,0)$ will depend upon the amplitude and the frequency of the ripples on supply lines, and the transfer functions of the stages will have the form:

$$(2a)\quad T_{PSR^+}(p) = \frac{U(201,0)}{V^+ \pm \Delta V^+} = k_{1.GPSR^+} R_{PSR^+}\left(1 + p\frac{L_{PSR^+}}{R_{PSR^+}}\right),$$

$$(2b)\quad T_{PSR^-}(p) = \frac{U(202,0)}{V^- \pm \Delta V^-} = k_{1.GPSR^-} R_{PSR^-}\left(1 + p\frac{L_{PSR^-}}{R_{PSR^-}}\right),$$

defining characteristics conditioned by one real zero. Signals generated at nodes (201,0) and (202,0) are used for forming the characteristic equation of E_{PSR} as follows:

$$(3)\quad U(E_{PSR}) = k_{0.EPSR} + k_{1.EPSR}U(201,0) + k_{2.EPSR}U(202,0).$$

The constant component $k_{0.ESR}$ in (3) determines the offset voltage U_{IO} of the op amp for the models of first level, and the coefficients $k_{1.ESR}$ and $k_{2.ESR}$ are used for modeling the change in U_{IO} as a result of changing the supply voltages ($V^+ \pm \Delta V^+$ or $V^- \pm \Delta V^-$). Then $PSRR^+$ and $PSRR^-$ will be determined by the following expressions:

(4a) $$PSRR^{+}(p)=\frac{A_{VD}}{A_{V^{+}}}=T(p)=\frac{U_{OUT}/U(205,0)}{U_{OUT}/(V^{+}\pm\Delta V^{+})}=\frac{\left(k_{1,GPSR^{+}}R_{PSR^{+}}\right)^{-1}}{k_{1,EPSR}\dfrac{L_{PSR^{+}}}{R_{PSR^{+}}}\left(p+\dfrac{R_{PSR^{+}}}{L_{PSR^{+}}}\right)}=\frac{H^{+}\omega_{p}^{+}}{p+\omega_{p}^{+}},$$

(4b) $$PSRR^{-}(p)=\frac{A_{VD}}{A_{V^{-}}}=T(p)=\frac{U_{OUT}/U(205,0)}{U_{OUT}/(V^{-}\pm\Delta V^{-})}=\frac{\left(k_{1,GPSR^{-}}R_{PSR^{-}}\right)^{-1}}{k_{2,EPSR}\dfrac{L_{PSR^{-}}}{R_{PSR^{-}}}\left(p+\dfrac{R_{PSR^{-}}}{L_{PSR^{-}}}\right)}=\frac{H^{-}\omega_{p}^{-}}{p+\omega_{p}^{-}}.$$

Comparing the last expressions leads to: $\omega_{P}^{+}=\dfrac{R_{PSR^{+}}}{L_{PSR^{+}}}$; $PSRR_{DC}^{+}=H=\left(k_{1,EPSR}k_{1,GPSR^{+}}R_{PSR^{+}}\right)^{-1}$;

$\omega_{P}^{-}=\dfrac{R_{PSR^{-}}}{L_{PSR^{-}}}$; $PSRR_{DC}^{-}=H^{-}=\left(k_{2,EPSR}k_{1,GPSR^{-}}R_{PSR^{-}}\right)^{-1}$.

These relationships are of basic importance for the methodology of determining the new characteristic parameters of the macromodel. Resistors R_{PSR}^{+} and R_{PSR}^{-} are selected of equal values: $R_{PSR}^{+}=R_{PSR}^{-}=100\Omega$. The low resistance value of 100Ω leads to minimization of the generated thermal noise. If necessary R_{PSR}^{+} and R_{PSR}^{-} could be represented by current sources controlled by their own voltages, thus conditioning noiseless resistors. For convenience, the coefficients $k_{1,ESR}$ and $k_{2,ESR}$ of the dependent source E_{PSR} are selected equal to unity. The coefficients of dependent sources $G_{PSR^{+}}$ and $G_{PSR^{-}}$ are obtained from the equations: $k_{1,GPS^{+}}=1/\left(R_{PSR^{+}}PSRR_{DC}^{+}\right)=10.10^{-9}\,S$ and $k_{1,GPS^{-}}=1/\left(R_{PSR^{-}}PSRR_{DC}^{-}\right)=5{,}623.10^{-9}\,S$. The inductivities $L_{PSR^{+}}$ and $L_{PSR^{-}}$ represent the decrease in $PSRR^{+}$ and $PSRR^{-}$ at high frequencies. These are calculated as follows: $L_{PSR^{+}}=R_{PSR^{+}}/\omega_{p}^{+}=2{,}653H$, and $L_{PSR^{-}}=R_{PSR^{-}}/\omega_{p}^{-}=1{,}4159H$, where $\omega_{p}^{+}=2\pi f_{p(PSR^{+})}$ and $\omega_{p}^{-}=2\pi f_{p(PSR^{-})}$ are the pole frequencies at level -3dB.

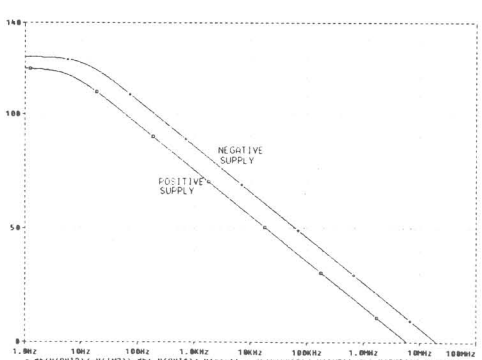

Fig. 3 OP-27 Simulated *PSRR* effects

The validation of the *PSRR* macromodel of an op amp is carried out by comparing the results of simulation modeling of OP-27/AD with technical sheet data of the real OP-27 op amp. To calculate the *PSRR* in relationship with the frequency requires that an alternated-current analysis (*AC Sweep*) be performed within the frequency range from 1 Hz to 10 MHz. Moreover, U_{IO} must be compensated for in advance. Fig. 3 shows the plotted results of the simulation modeling of $PSRR^{+}$ and $PSRR^{-}$ for OP-27/AD-PSR. The comparison gives a very good agreement between the macromodel created and the real op amp, the resulting error being within 2,5 %.

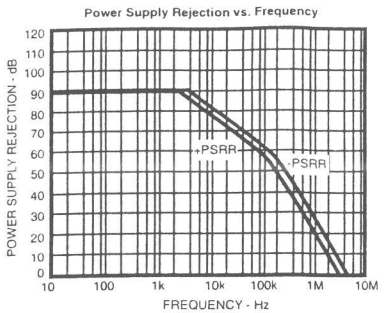

Fig. 4. AD820 *PSRR* effects

2.2 Two-pole approximation of the frequency characteristic of PSRR.

There exist op amps for which the frequency characteristic of PSRR can be approximated by a transfer function of second order determined by a pair of real poles. Such characteristics of *PSRR* depending on the frequency of positive and negative supply voltages are shown in Fig. 4 (*Analog Devices* AD820). The maximal values of *PSRR* at frequency 10 *Hz* are: $PSRR^{+}_{DC} = PSRR^{-}_{DC} = 31622$. The frequencies for the first and second poles are $f_{p1(PSR^{+})} = 2{,}2kHz$, $f_{p2(PSR^{+})} = 110kHz$ and $f_{p1(PSR^{+})} = 4kHz$, $f_{p2(PSR^{-})} = 120kHz$, respectively. In ranges $f_{p1(PSR^{+})} < f < f_{p2(PSR^{+})}$ and $f_{p1(PSR^{-})} < f < f_{p2(PSR^{-})}$ the characteristics slope is -20*dB/dec*.

The development of the macromodels of first, second and third levels has been performed by analogy to the previous case. As it is shown in Fig. 5 the equivalent circuits of the macromodels of different complexity levels are modified by adding two more stages determining the second pole in the frequency characteristic of *PSRR*. The additionally

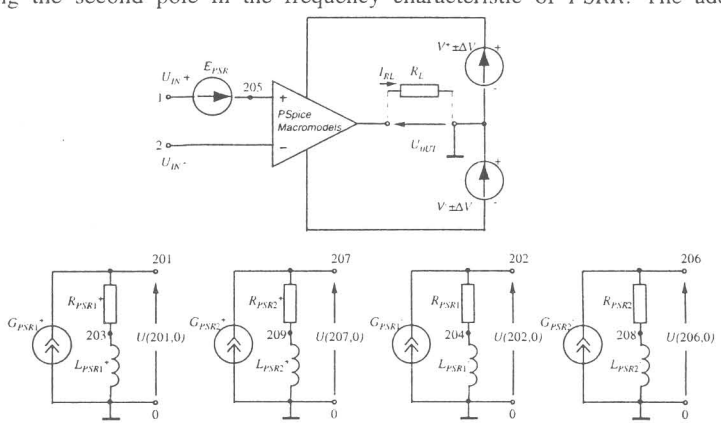

Controlled sources functions

$$I(G_{PSR1^{+}}) = k_{1,GPSR1^{+}} V^{+} \quad I(G_{PSR1^{-}}) = k_{1,GPSR1^{-}} V^{-}$$

$$I(G_{PSR2^{+}}) = k_{1,GPSR2^{+}} U(201,0) \quad I(G_{PSR2^{-}}) = k_{1,GPSR2^{-}} U(202,0)$$

$$U(E_{PSR}) = k_{0,EPSR} + k_{1,EPSR} U(206,0) + k_{2,EPSR} U(207,0)$$

Fig. 5. Modified circuit op amp of macromodel for presenting second-order *PSRR* function

defined stages of the macromodel consist of the dependent sources $G_{PSR2^{+}}$ and $G_{PSR2^{-}}$ and frequency-determining *RL*-groups: $R_{PSR2^{+}}$, $L_{PSR2^{+}}$ and $R_{PSR2^{-}}$, $L_{PSR2^{-}}$. The source $G_{PSR2^{+}}$ presets the voltage at node 207 that depends on the voltage (202,0). To provide an accuracy sufficient for the process of modeling the dependent current sources have been selected as

linear one-port sources with characteristic equations in accordance with Fig. 5. Then $PSRR^+$ and $PSRR^-$ are determined by the following expressions:

$$(5a)\quad PSRR^+(p)=\frac{A_{VD}}{A_{V^+}}=\frac{1}{k_{1.EPSR}T_{PSR^+}(p)}=\frac{\left(k_{1.GPSR1^+}.R_{PSR1^+}\right)^{-1}}{k_{1.EPSR}\left(1+p\dfrac{L_{PSR1^+}}{R_{PSR1^+}}\right)}.\frac{\left(k_{1.GPSR2^+}.R_{PSR2^+}\right)^{-1}}{\left(1+p\dfrac{L_{PSR2^+}}{R_{PSR2^+}}\right)}$$

$$(5b)\quad PSRR^-(p)=\frac{A_{VD}}{A_{V^-}}=\frac{1}{k_{2.EPSR}T_{PSR^-}(p)}=\frac{\left(k_{1.GPSR1^-}.R_{PSR1^-}\right)^{-1}}{k_{2.EPSR}\left(1+p\dfrac{L_{PSR1^-}}{R_{PSR1^-}}\right)}.\frac{\left(k_{1.GPSR2^-}.R_{PSR2^-}\right)^{-1}}{\left(1+p\dfrac{L_{PSR2^-}}{R_{PSR2^-}}\right)}.$$

The new defined macromodel parameters can be obtained by using the following equations

$$\begin{aligned}
&R_{PSR1^+}=R_{PSR2^+}=R_{PSR1^-}=R_{PSR2^-}=100\Omega;k_{1.GPSR1^+}=1/(PSRR^+_{DC}.R_{PSR1^+})=316{,}22776nS,\\
&k_{1.GPSR2^+}=1/R_{PSR2^+})=10mS;k_{1.GPSR1^-}=1/(PSRR^-_{DC}.R_{PSR1^-})=316{,}22776nS,\\
(6)\quad &k_{1.GPSR2^-}=1/R_{PSR2^-})=10mS;L_{PSR1^+}=R_{PSR1^+}(2\pi f_{P1(PSR^+)})=7{,}238mH,\\
&L_{PSR2^+}=R_{PSR2^+}(2\pi f_{P2(PSR^+)})=144{,}76\mu H;L_{PSR1^-}=R_{PSR1^-}(2\pi f_{P1(PSR^-)})=3{,}981mH,\\
&L_{PSR2^-}=R_{PSR2^-}(2\pi f_{P2(PSR^-)})=132{,}69\mu H;k_{1.EPSR}=k_{2.EPSR}=1,
\end{aligned}$$

where $f_{P1(PSR^+)}$, $f_{P2(PSR^+)}$ are the first and second pole frequencies of the $PSRR^+$, respectively, and $f_{P1(PSR^-)}$, $f_{P2(PSR^-)}$ the first and second pole frequencies of the $PSRR^-$, respectively.

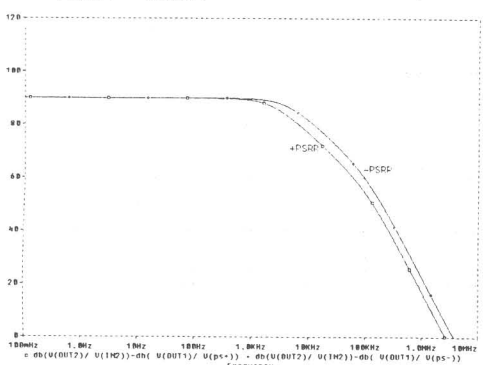

Fig. 6. AD820/AD Simulated *PSRR* effects

Verification checks, have been performed on the *PSRR* macromodels developed by using Analog Devices JFET low noise, precision op amp AD820 [8]. Simulation testing has been carried out for the open-loop amplifier and compensated DC value of the input offset voltage. For the last case we have given an example with op amp AD820 where the *PSRR* frequency characteristics are approximated as a second-order transfer function. The results of this simulation together with the experimental curves (data sheet) are shown in Figure 4 and 6. The first and second poles of the *PSRR* response have been simulated quite well. Results obtained from these computer simulations demonstrate good agreement (better than 3%).

2.3. Approximating the frequency characteristic of PSRR by a transfer function determined by one pole/zero pair. Analyzing the frequency characteristics of *PSRR* shown in Fig. 7 (*Burr-Brown* OPA620) leads to the conclusion that the frequency characteristic of *PSRR* can be represented, with an accuracy sufficient for the practice, as a transfer function determined by one pole/zero pair. The maximal values of *PSRR* at frequency 1 *kHz* are: $PSRR^+_{DC}=1{,}778.10^3$ and $PSRR^-_{DC}=1.10^3$. And the frequencies of pole/zero pairs are

$f_{P(PSR^+)} = 1MHz$, $f_{P(PSR^-)} = 320kHz$ и $f_{Z(PSR^+)} = 400MHz$, $f_{Z(PSR^-)} = 180MHz$, respectively. In ranges $f_{P(PSR^+)} < f < f_{Z(PSR^+)}$ and $f_{P(PSR^-)} < f < f_{Z(PSR^-)}$ the characteristics slope is -20*dB/dec*.

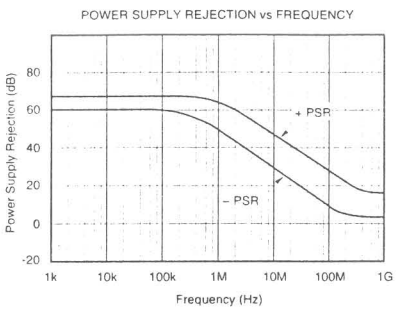

Fig. 7. OPA620 *PSRR* effects

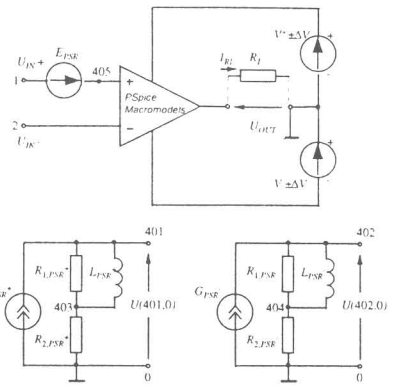

Fig. 8. Modified circuit op amp of macromodel for presenting first-order pole/zero *PSRR* function

The development of the models of first, second and third levels is performed by analogy to the previous consideration where *PSRR* has been approximated by a transfer function with one pole. As it is shown in Fig. 8 the equivalent circuits of the existent macromodels of different complexity levels are modified. Connecting the linear two-port voltage-controlled dependent voltage source E_{PSR} into the input circuit of the macromodel engenders a new node 405 the state of which should follow the variation of the input voltage of asymmetry modeling the *PSRR*. the additionally defined stages of the macromodel consist of the dependent sources G_{PSR^+} and G_{PSR^-} and frequency-determining *RL*-groups: R_{PSR1^+}, R_{PSR2^+}, L_{PSR^+} and R_{PSR1^-}, R_{PSR2^-}, L_{PSR^-}. The source G_{PSR^+} presets the voltage at node 401 that depends on ripples of supply voltage ($V^+ \pm \Delta V^+$), and G_{PSR^-} forms the voltage at node 402 depending on ripples of the negative supply voltage ($V^- \pm \Delta V^-$). To provide an accuracy sufficient for the process of modeling the sources G_{PSR^+} и G_{PSR^-} have been selected as linear one-port sources with characteristic equations (1a) and (1b). The transfer functions of these stages are:

$$(7a) \quad T_{PSR^+}(p) = \frac{U(401,0)}{V^+ \pm \Delta V^+} = k_{1.GPSR^+} R_{PSR2^+} \frac{R_{PSR1^+} + pL_{PSR^+}\left(1 + R_{PSR1^+} / R_{PSR2^+}\right)}{R_{PSR1^+} + pL_{PSR^+}}$$

$$(7b) \quad T_{PSR^-}(p) = \frac{U(402,0)}{V^+ \pm \Delta V^-} = k_{1.GPSR^-} R_{PSR2^-} \frac{R_{PSR1^-} + pL_{PSR^-}\left(1 + R_{PSR1^-} / R_{PSR2^-}\right)}{R_{PSR2^-} + pL_{PSR^-}}$$

Equations (7a) and (7b) define characteristics that are determined by one pole/zero pair. The frequency-dependent voltages at nodes (401,0) and (402,0) will participate as second and third components, respectively, in the characteristic equation of the source E_{PSR}:

$$(8) \quad U(E_{PSR}) = k_{0.EPSR} + k_{1.EPSR} U(401,0) + k_{2.EPSR} U(402,0).$$

Then $PSRR^+$ and $PSRR^-$ will be determined by the following expressions:

$$(9a)\quad PSRR^{+}(p)=\frac{A_{VD}}{A_{V^+}}=\frac{U_{OUT}/U(405,0)}{U_{OUT}/V^{+}}=\frac{\left(k_{1,EPSR}k_{1,GPSR^+}R_{PSR2^+}\right)^{-1}\left(R_{PSR2^+}+pL_{PSR^+}\right)}{R_{PSR1^+}+pL_{PSR^+}\left(1+R_{PSR1^+}/R_{PSR2^+}\right)},$$

$$(9b)\quad PSRR^{-}(p)=\frac{A_{VD}}{A_{V^-}}=\frac{U_{OUT}/U(405,0)}{U_{OUT}/V^{-}}=\frac{\left(k_{2,EPSR}k_{1,GPSR^-}R_{PSR2^-}\right)^{-1}\left(R_{PSR1^-}+pL_{PSR^-}\right)}{R_{PSR1^-}+pL_{PSR^-}\left(1+R_{PSR1^-}/R_{PSR2^-}\right)},$$

The model parameters are calculated as follows:

$$R_{PSR2^+}=R_{PSR2^-}=1k\Omega;k_{1,GPSR^+}=1/(PSRR^{+}_{DC}.R_{PSR2^+})=562{,}34nS;k_{1,GPSR^-}=1/(PSRR^{-}_{DC}.R_{PSR2^-})=1\mu S;$$

$$R_{PSR1^+}=R_{PSR2^+}(f_{Z(PSR^+)}/f_{P(PSR^+)}-1)=399k\Omega;\ L_{PSR^+}=R_{PSR1^+}/(2\pi f_{Z(PSR^+)})=158{,}84\mu H;$$

$$R_{PSR1^-}=R_{PSR2^-}(f_{Z(PSR^-)}/f_{P(PSR^-)}-1)=561{,}5k\Omega;\ L_{PSR^-}=R_{PSR1^-}/(2\pi f_{Z(PSR^-)})=496{,}73\mu H$$

$$k_{1,EPSR}=k_{2,EPSR}=1,$$

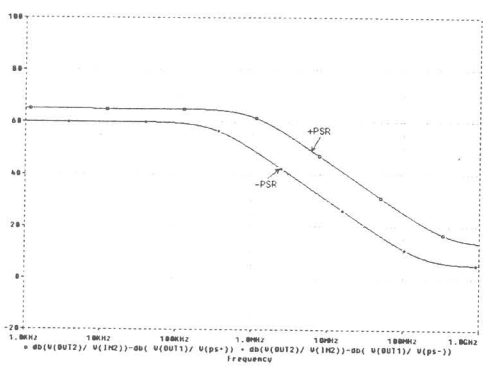

Fig.9. OPA620/BB-PSR Simulated *PSRR* effects

Verification checks have been performed on the PSRR macromodels developed by using Burr-Brown wide-band, precision op amp OPA620 [7], for which the frequency characteristic of *PSRR* has been approximated as a first-order pole/zero function. Figures 7 and 9 demonstrate *PSRR* functions of the actual OPA620 and its model, respectively, the resulting error being not higher than 4%.

3. Conclusion

This paper presents new developments of op amp simulation *PSpice*-macromodels aimed at improving the power supply rejection ratio versus frequency. The models developed have been implemented as sub-circuits, and the structure of their netlists conforms to the *PSpice* format. Despite the addition of all these new features, the macromodel's simulation speed and computation memory needed are still equal to those of the *PSpice* standard library models.

References

[1] Shoikova E., I. Pandiev: "*PSpice Macromodels of Operational Amplifiers*", TUS, Sofia, 2000.

[2] "Operational Amplifier Macromodels", Texas Instruments Application Brief, 1994.

[3] Bowers D., A. Mark, "Spice-Compatible Op Amp Macromodels", *EDN*, February 1990, pp. 143-154.

[4] Hu, C., D. Leach, S. Chan, "An Improved Macromodel for Operational Amplifiers", *International Journal of Circuit Theory and Applications*, Vol. 18, pp.189-203, 1990.

[5] Laker, K., W. Sansen: "*Design of Analog Integrated Circuits and Systems*", McGraw-Hill, 1994.

[6] Shoikova, E., I. Pandiev, "Macromodeling of Operational Amplifier's Temperature Effects", *SIITME, Conference Proceedings*, pp. 59-63, *September* 2000.

[7] Burr-Brown IC Data Book, 1998.

[8] Design-In Reference Manual, Analog Devices, 1994.